ACS NANO
Cite This: ACS Nano XXXX, XXX, XXX−XXX
www.acsnano.org

ARTICLE

Plasmonic Resonance Enhanced Polarization-Sensitive Photodetection by Black Phosphorus in Near Infrared

Prabhu K. Venuthurumilli,[†] Peide D. Ye,[‡] and Xianfan Xu*[,†,‡]

[†]School of Mechanical Engineering and Birck Nanotechnology Center, Purdue University, West Lafayette, Indiana 47907, United States

[‡]School of Electrical and Computer Engineering, Purdue University, West Lafayette, Indiana 47907, United States

Supporting Information

ABSTRACT: Black phosphorus, a recently intensely investigated two-dimensional material, is promising for electronic and optoelectronic applications due to its higher mobility and thickness-dependent direct band gap. With its low direct band gap and anisotropic properties in nature, black phosphorus is also suitable for near-infrared polarization-sensitive photodetection. To enhance photoresponsivity of a black phosphorus based photodetector, we demonstrate two designs of plasmonic structures. In the first design, plasmonic bowtie antennas are used to increase the photocurrent, particularly in the armchair direction, where the optical absorption is higher than that in the zigzag direction. The simulated electric field distribution with bowtie structures shows enhanced optical absorption by localized surface plasmons. In the second design, bowtie apertures are used to enhance the inherent polarization selectivity of black phosphorus. A high photocurrent ratio (armchair to zigzag) of 8.7 is obtained. We choose a near-infrared wavelength of 1550 nm to demonstrate the photosensitivity enhancement and polarization selectivity, as it is useful for applications including telecommunication, remote sensing, biological imaging, and infrared polarimetry imaging.

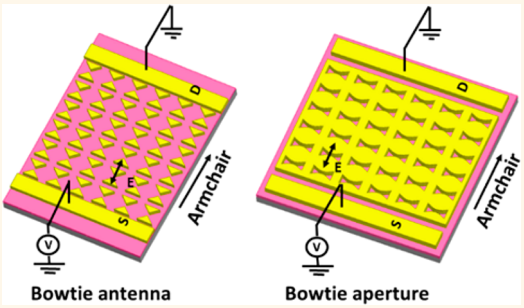

KEYWORDS: *black phosphorus, plasmonics, polarization-sensitive, near-infrared, photodetector, bowtie antenna, bowtie aperture*

Two-dimensional materials are of immense interest due to their extraordinary properties compared to their bulk counterparts. In addition to graphene[1,2] and transition metal dichalcogenides[3,4] such as MoS_2,[5,6] few-layer black phosphorus (BP) is intensively studied recently due to its unique properties including high mobility[7] and a thickness-dependent direct band gap, ∼0.3 eV in bulk and around 1.5 eV in monolayer,[8−12] whereas MoS_2 has a direct band gap only as a monolayer.[13,14] Well-behaved field effect transistors in BP have been demonstrated.[15,16] With these extraordinary properties, BP is a promising candidate for electronic and optoelectronic applications including scaled high-performance transistors,[17] solar cells,[18] and photodetectors.[19,20]

The unique thickness-dependent direct band gap makes BP especially promising for photodetection. In this work we investigate methods to enhance photoresponse in black phosphorus photodetectors at near-IR wavelength, which can find use in various applications including telecommunication, remote sensing, and biological imaging.[21] Conventional IR detectors require either an expensive fabrication process such as molecular beam epitaxy, low-temperature operation, or both. Moreover, integration of these conventional narrow band gap semiconductors with traditional electronic materials such as silicon is difficult due to lattice mismatch.[22] In contrast, the layered structure of black phosphorus is suitable for monolithic integration with silicon and even with flexible substrates.[23] BP photodetectors have been reported.[16,19,20,24−26] However, the performance of most of these photodetectors is limited because of low light absorption in thin films. On the other hand, plasmonic structure enhanced photoresponsivity at visible wavelengths has been demonstrated in graphene[27,28] and MoS_2.[29] Here, we demonstrate enhanced photosensitivity and polarization selectivity in BP using plasmonic structures at the near-IR wavelength of 1550 nm. The same methods can be used for longer wavelengths up to the band gap of BP, ∼4 μm.[11] We report two designs of plasmonic structures to enhance photosensitivity and polarization-sensitive photodetection. In the first design, we use bowtie antennas to enhance absorption and hence the photocurrent. Computational design shows that the enhanced absorption is due to field

Received: March 4, 2018
Accepted: April 23, 2018
Published: April 23, 2018

DOI: 10.1021/acsnano.8b01660
ACS Nano XXXX, XXX, XXX−XXX

enhancement by bowtie plasmonic structures. In the second design, we use bowtie apertures (or bowtie aperture antennas) to enhance the inherent polarization selectivity of BP. BP has a puckered layer structure, resulting in anisotropic in-plane properties[30−32] along its two principal armchair and zigzag directions including anisotropic optical properties, where the armchair direction has greater absorption compared to that along the zigzag direction.[26,33,34] Inversion symmetry and mirror reflection symmetry of a crystal structure in the zigzag direction forbid transitions of photons polarized in the zigzag direction with band gap energy and significantly reduce absorption of photons with higher energies.[26] The transmission of light through bowtie apertures is also polarization dependent[35] and hence can further enhance the polarization selectivity of BP. Here we experimentally demonstrate a bowtie aperture enhanced BP detector with a photocurrent ratio (armchair to zigzag) of 8.7, which is useful in IR polarimetry imaging.[36]

RESULTS AND DISCUSSION

BP flakes are prepared by tape exfoliation from bulk onto a SiO_2/Si substrate (see Methods). In the first design, we use bowtie antenna plasmonic structures to enhance the photoresponse. Figure 1a shows an optical image of two devices on

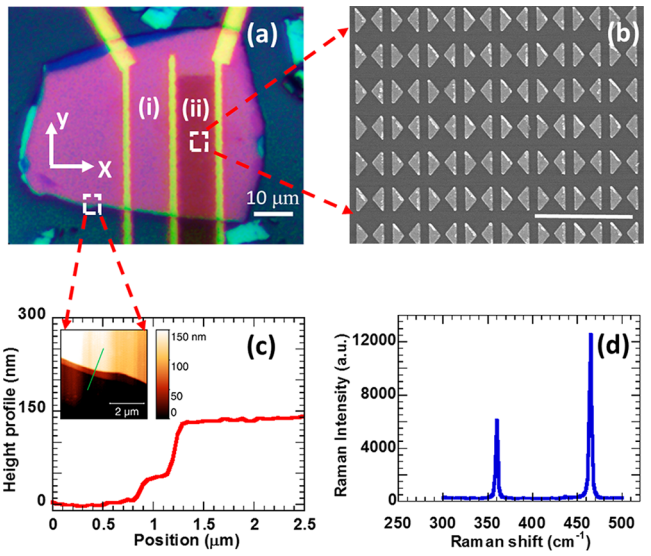

Figure 1. Bowtie antenna BP photodetector. (a) Optical image of two BP devices on one flake, (i) without plasmonic nanostructures and (ii) with an array of bowtie antennas. (b) SEM image of an array of bowtie antenna structures. Scale bar is 2 μm. (c) AFM height profile across the boundary of the BP flake (green line in the inset). Inset shows the AFM topography image of the BP flake. (d) Polarized Raman spectra for identifying the armchair direction in BP (the *x*-direction in Figure 1a).

the same flake: (i) without plasmonic structures and (ii) with bowtie antenna plasmonic structures. The plasmonic structures and contacts are fabricated using standard e-beam lithography, metallization, and lift-off processes. Thin-film metal of Ti/Au (5 nm/75 nm) is deposited for both the plasmonic structures and contacts. A scanning electron microscopy (SEM) image of the bowtie structures of device (ii) in Figure 1a is shown in Figure 1b. The flake is 135 nm thick, as characterized by atomic force microscopy (AFM), and is shown in Figure 1c. Polarized Raman spectroscopy is used to determine the lattice orientation of BP.[31] Figure 1d shows the Raman spectrum when the polarization is along the *x*-direction (Figure 1a), indicating that the *x*-direction is the armchair direction.[31] The device channel lengths (as seen in Figure 1a) are designed along the armchair direction for better photocarrier collection. This is because of shorter carrier transit time due to higher mobility along the armchair direction than that along the zigzag direction.[20] The absorption of BP is also stronger along the armchair direction as compared to the zigzag direction.[26,31] Hence, the bowtie structures are aligned by fabricating along the armchair direction as shown in Figure 1b to enhance armchair absorption by the localized surface plasmons.

To study the photoresponse of the devices, scanning photocurrent measurements are first conducted on the devices with zero bias. The photocurrent map at zero bias and 470 μW incident power at 1550 nm wavelength of the device with plasmonic structures is shown in Figure 2a. The laser spot size

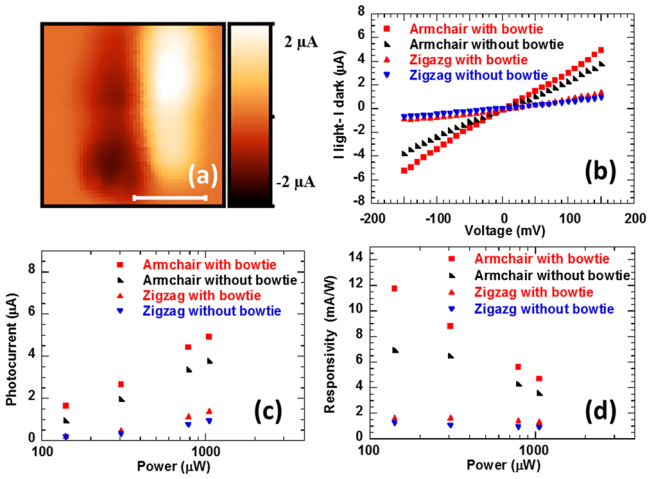

Figure 2. Response of the BP photodetector at 1550 nm wavelength. (a) Photocurrent map of the device with plasmonic structures at zero bias, with 470 μW incident laser power. Scale bar is 20 μm. (b) Illumination current minus dark current ($I_{light} - I_{dark}$) *vs* bias voltage at 1.05 mW of laser power for both devices, with and without bowtie antennas, and both polarizations along armchair and zigzag directions. (c) Photocurrent *vs* laser power at 150 mV bias. (d) Photoresponsivity *vs* laser power at 150 mV bias.

is about 4.7 μm. We see two current lobes of different sign at the two contacts. This is due to the photothermoelectric effect[37] and band bending at the contacts, which were observed in MoS_2[38] and other BP devices.[19] Recent studies on graphene,[39] carbon nanotubes,[40,41] and MoS_2[38] show that the photothermoelectric effect may play an important role in the photoresponse. To study the effect of the plasmonic structures alone, all the subsequent photocurrent measurements are performed at the zero current point of zero bias, which is located near the center of the devices, and results are shown in Figure 2(b−d). The dark current (without incident light) *I*−*V* curves of both devices are shown in Supplementary Figure S1. We observe that devices are nonrectifying, and small nonlinearity could be due to the Schottky barrier. Under laser illumination, the photocurrent (current under illumination minus dark current) *vs* bias at a laser power of 1.05 mW is shown in Figure 2b for both devices and for polarizations along armchair and zigzag directions. We can see clearly that the photocurrent in the device with bowtie structures is much larger than that in the device without structures because of enhanced absorption by plasmonic structures. Also, the

DOI: 10.1021/acsnano.8b01660
ACS Nano XXXX, XXX, XXX−XXX

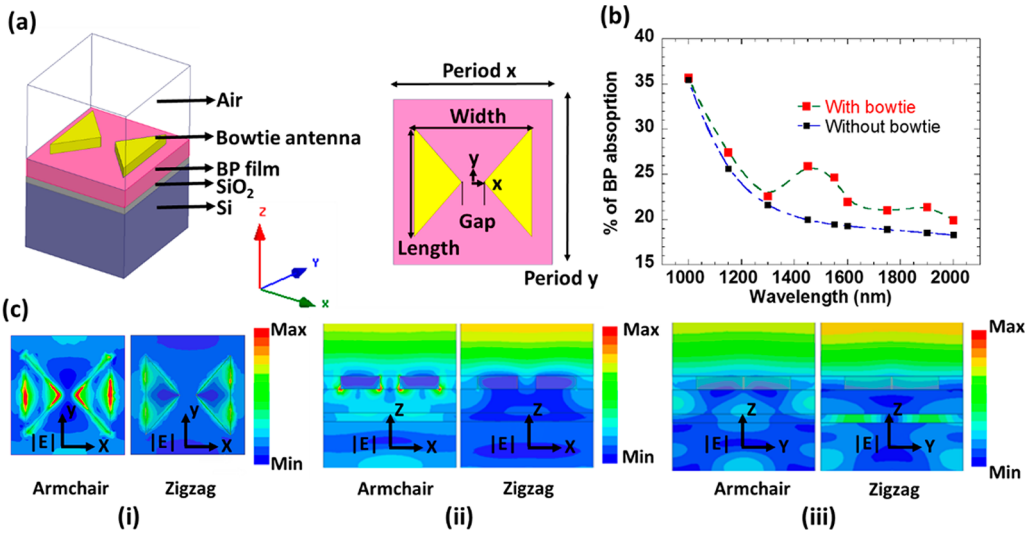

Figure 3. Simulated response of a BP device with a bowtie antenna array. (a) Schematic of a unit cell of the simulation model. (b) Calculated absorption in BP, with and without bowtie structures, when illuminated along the armchair direction. (c) Electric field distributions: (i) top view of the XY plane at the exit of the bowtie antenna, (ii) cross-sectional view of the XZ plane, and (iii) cross-sectional view of the YZ plane, for illuminations along the armchair and zigzag directions at 1550 nm wavelength.

photocurrent when illuminated along the armchair direction is larger than that along the zigzag direction due to higher absorption in BP and higher transmission through bowtie antennas. The photocurrent increases with bias because of extraction of more electron−hole pairs before they are recombined. The photocurrent *vs* laser power at 150 mV bias is shown in Figure 2c for both devices and illumination polarizations. The photocurrent increases with laser power because of generation of more electron hole pairs. The photoresponsivity, defined as photocurrent divided by laser power, at 150 mV bias is shown in Figure 2d. The photoresponsivity decreases with increasing laser power, which is a common behavior of photodetectors due to saturation of the electron−hole pair generation at high laser power and the increased surface recombination.[42]

Plasmonic structures were optimized using the finite element electromagnetic solver ANSYSEM at the wavelength of 1550 nm for absorption along the armchair direction, along which inherent absorption of BP is higher (see Methods). A schematic of the model is shown in Figure 3a. Light is illuminated from the air side (from the top in Figure 3a), the bowtie structures are aligned along the armchair direction (the x direction in Figure 3a) of BP, and the enhanced absorption of BP by bowtie structures along the armchair direction is shown in Figure 3b. The decreasing absorption in BP *vs* wavelength for the case without bowties is because of thin-film interference. The simulated electric field distributions with the fabricated bowtie structure dimensions (length = 524 nm, width = 563 nm, gap = 107 nm, period x = 758 nm, and y = 790 nm) are shown in Figure 3c. From the field distributions in the XY plane at the exit of bowtie antenna and in the cross-section of the XZ plane, we see the enhancement of the electric field in BP at the tip of the bowtie antennas for illumination along the armchair direction. This field enhancement in BP caused by bowtie structures leads to the increase in absorption.

The experimental results on photocurrent are generally in agreement with simulation results of light absorption in BP. The absorption in both the polarizations is increased because of field enhancement by plasmonic structures. From the simulations, absorption in the armchair direction is increased from 19% in the device without structures to 25% in the device with structures (a 32% increase), while the absorption in the zigzag direction is increased from 2% in the device without structures to 4% in a device with structures (a 100% increase). We see from Figure 2b that the measured photocurrent increases with plasmonic structures for both polarizations, and the photocurrent when illuminated along the armchair direction is higher than that along the zigzag polarization. With a laser power of 1.05 mW and 150 mV bias, the photocurrent enhancement is about 31% along the armchair direction and 50% along the zigzag direction. At a lower laser power of 130 μW (and the same 150 mV bias), the photocurrent enhancement is about 70% along the armchair direction and 37% along the zigzag direction. We cannot draw a quantitative comparison between the simulated electric field distributions and the experimental photocurrent measurements. The photocurrent depends on extraction of electron hole pairs and is affected by electron hole recombination, while the simulations only show the absorbed electric field.

The maximum photocurrent occurs near the electrodes. The maximum photocurrent with plasmonic structures is also larger than that in the device without plasmonic structures, as shown in Supplementary Figure S2. The maximum photoresponsivity for the armchair polarization with plasmonic structures is 14.2 mA/W at a laser power of 470 μW and 100 mV bias and has an increase of 43% and 61% for armchair and zigzag polarizations, respectively, compared with those without plasmonic structures. As a comparison, the responsivities at a wavelength of 1550 nm by previous studies are 0.3 mA/W (at the same bias of 100 mV)[26] and 3 mA/W (at our incident power for measurements performed up to 200 mV bias).[19] Therefore, the responsivity of our plasmonic-enhanced BP photodetector is more than 4 times greater than the previously reported values. In addition to enhanced absorption in BP by plasmonic structures, there is a built-in field at the interface of BP and Ti/Au structures caused by the work function difference, which separates the photoinduced carriers generated in BP. The electrons will be swept from the surface of BP into the metal,

DOI: 10.1021/acsnano.8b01660
ACS Nano XXXX, XXX, XXX−XXX

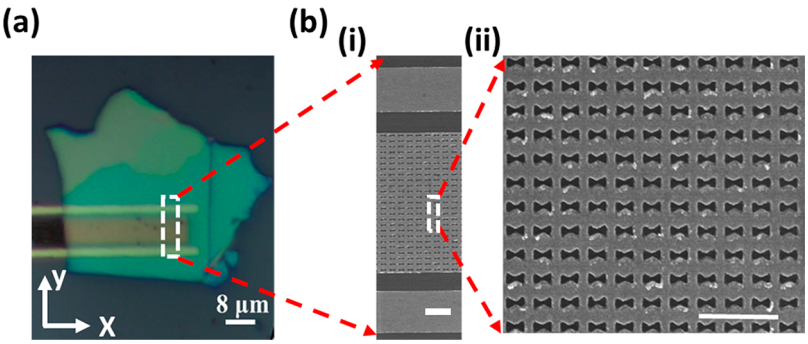

Figure 4. Bowtie aperture BP photodetector. (a) Optical image of the BP photodetector with the array of bowtie apertures. (b) (i) SEM image of an array of bowtie apertures and contacts on the BP flake. Scale bar is 1 μm. (ii) Zoomed-in image of the array of bowtie apertures. Scale bar is 1 μm.

while there is a small barrier for holes as seen from the band diagram.[16] This can lead to longer recombination time and can cause more photocurrent, as was observed in graphene.[43,44] Also, very limited photocurrent was reported by hot electrons from gold plasmonic structures injected into silicon over the Schottky barrier.[45] In our experiments, we are unable to distinguish the contribution between the hot electrons from metal and photoinduced carriers in BP, as our incident energy is greater than the band gap of BP. However, we expect the hot electron contribution to be weak, as there is no barrier for electrons to return to the gold by the built-in field at the interface.

We performed the transient current measurements by mechanically modulating the incident light. However, we are limited by the frequency of the mechanical chopper to obtain the actual response time of devices as shown in the Supplementary Figure S3. From our measurements, the response time of the devices, with and without bowtie structures, is less than 90 μs, for light polarization along armchair and zigzag directions. The reported intrinsic response time of the black phosphorus photodetector can be as fast as ~75 ps along both armchair and zigzag directions.[46] Since we expect the hot electron contribution to be weak, the response time of devices with and without plasmonic structures would be similar to those observed in graphene.[43]

In the second design, we use an array of bowtie apertures to enhance the polarization selectivity of BP photodetection. Just to compare, the first design of bowtie antennas is intended to enhance the photocurrent; however, the polarization ratio (defined as the ratio of photocurrent in the armchair direction to that in the zigzag direction) is not increased much, as shown in the Supplementary Figure S4. The inherent absorption of BP is higher along the armchair polarization than the zigzag direction.[26,31] The transmission of light through bowtie apertures also depends on the incident polarization, and the transmission along the direction of the gap of the bowtie aperture is higher.[35] Hence, the second design of bowtie apertures enhances the absorption ratio by suppressing transmission for polarization along the zigzag direction, as there is no BP exposed to light other than that through the apertures. In our design, the bowtie aperture gaps are aligned along the armchair direction to take advantage of the higher absorption along the armchair direction. Figure 4a shows an optical image of the device with the array of bowtie apertures, and Figure 4b shows an SEM image of bowtie apertures. The armchair direction in this device is along the *y* direction of Figure 4a, as determined by the polarized Raman spectroscopy.[31] The flake is 95 nm thick as characterized by AFM and is shown in Supplementary Figure S5. The device channel length is again designed along the armchair direction because of higher mobility along the armchair direction, as was done for the previous design.

All photocurrent measurements are conducted at the zero current point at 0 V bias, and the results are shown in Figure 5.

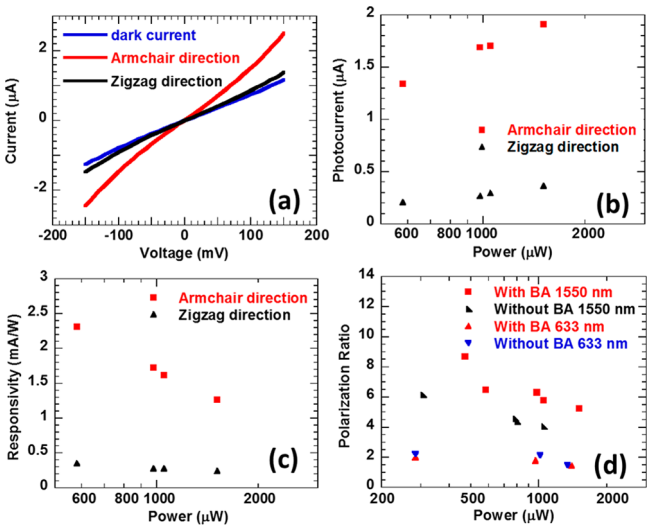

Figure 5. Response of the bowtie apertures. (a) Dark current and illumination current at 580 μW *vs* voltage for different polarizations at 1550 nm. (b) Photocurrent *vs* power at 150 mV bias for different polarizations at 1550 nm. (c) Responsivity *vs* power at 150 mV bias for different polarizations at 1550 nm. (d) Comparing polarization ratio *vs* laser power at 150 mV bias, with and without bowtie apertures (BA) and at wavelengths of 1550 and 633 nm.

I−*V* curves of dark current (without incident light) and with a laser power of 580 μW (1550 nm wavelength) along armchair and zigzag polarizations are shown in Figure 5a. Photocurrent and photoresponsivity *vs* laser power at 150 mV bias are shown in Figure 5b and c, respectively, for both polarizations. Same as the previous device, the photocurrent increases with laser power, and photoresponsivity decreases with laser power due to the reasons discussed previously. The polarization ratio is shown in Figure 5d, as a function of laser power at 150 mV bias for devices with and without bowtie apertures. We see that the polarization ratio in the device with bowtie apertures increased from 4 to 5.8 (at a laser power of 1.05 mW) compared to that without bowtie apertures. The polarization ratio decreases with

DOI: 10.1021/acsnano.8b01660
ACS Nano XXXX, XXX, XXX−XXX

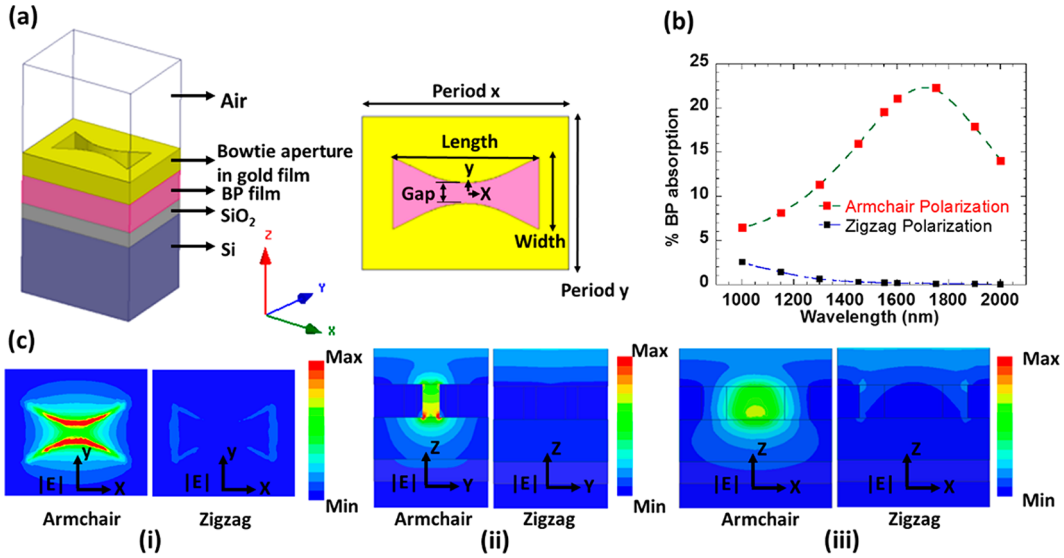

Figure 6. Simulated response of a BP device with an array of bowtie apertures. (a) Schematic of a unit cell of the simulation model. (b) Calculated absorption in BP with the fabricated dimensions for two different polarizations, armchair (along the *y* direction of Figure 6a) and zigzag (along the *x* direction of Figure 6a). (c) Electric field distributions: (i) top view of the XY plane at the exit of the bowtie aperture, (ii) cross-sectional view of the YZ plane, and (iii) cross-sectional view of the XZ plane for illuminations along the armchair and zigzag directions.

laser power both with and without bowtie apertures. The possible reason for the decrease in polarization ratio with increase in laser power is the saturation of increased photocurrent extraction in the armchair direction as the photoabsorption increases. At a lower laser power of 470 μW, a higher polarization ratio of 8.7 is obtained in the bowtie aperture BP photodetector. $I-V$ curves obtained at the laser power of 470 μW for both polarization directions are shown in Supplementary Figure S6. Also shown in Figure 5d is the measurement using a 633 nm wavelength. It is seen that the polarization ratio at 633 nm does not change much, as the response of the bowtie aperture strongly depends on the wavelength due to its plasmonic resonance. It was reported that patterned Au nanostructures can locally influence the graphene Fermi energy.[47,48] We do not expect Au patterns to strongly influence the transport properties in our devices of bulk BP. In our first device, although 20% of BP is covered by metal, the dark currents of both devices (with and without bowties) are similar, as shown in Supplementary Figure 1. For the second design, resistivity of the device with bowtie apertures is estimated to be 4.71 Ω cm, while the resistivity of the device without plasmonic structures shown in Figure 1 is 5.28 Ω cm. The 10% variation in resistivity could be because of device-to-device variation as well as a minor surface effect by gold.

BP photodetectors with bowtie apertures shown in Figure 4 were also designed using numerical simulation. A schematic of the simulation model is shown in Figure 6a. The plasmonic structures were designed such that the absorption ratio of armchair to zigzag is higher at a wavelength of 1550 nm. The fabricated device geometry is used in the results shown in Figure 6, with length = 247 nm, width = 122 nm, gap = 35 nm, period x = 349 nm, and period y = 259 nm. The gaps of bowtie aperture structures are aligned along the armchair direction (the y direction in Figures 4a and 6a) of BP. Light is illuminated from the air side, and absorption *vs* wavelength is shown in Figure 6b for polarizations along armchair and zigzag directions. At the resonance wavelengths (including 1550 nm), large absorption along the armchair direction results in higher polarization selectivity. From Figure 6b, we see that the absorption ratio of armchair to zigzag is expected to be high at the designed wavelength of 1550 nm. The electric field distributions across different planes, the XY plane at the exit of bowtie aperture and the cross-sectional YZ and XZ planes, for illuminations along the armchair and zigzag directions at wavelength of 1550 nm are shown in Figure 6c. From the field distributions, we clearly see the enhancement of electric field only for the armchair polarization by bowtie apertures. High transmission only in the armchair direction leads to the high polarization ratio of absorption. The resonant wavelength of the bowtie aperture plasmonic structures can be controlled by their dimensions, particularly the length of the bowtie aperture,[49] as shown in the Supplementary figure S7. The resonant wavelength increases with the length of the bowtie aperture, providing polarization selectivity at different wavelengths.

Bowtie apertures do not increase absorption for the armchair direction as compared to the device without bowtie apertures. Computations show absorption in the armchair direction is 19% with bowtie apertures as compared to 21% without bowtie apertures. On other hand, the absorption in the zigzag direction has decreased from 10% to less than 1% with bowtie apertures. The enhancement of the absorption ratio at the designed wavelength of 1550 nm from simulation is larger than the obtained experimental enhancement of the polarization ratio. The deviation can be due to factors including high sensitivity of resonance with dielectric constants (as shown in Supplementary Notes 8 and 9) and imperfections of the fabricated geometry of plasmonic structures (*e.g.*, variations in the sizes of fabricated bowtie apertures). In addition, we cannot draw a direct quantitative comparison between the simulated field distributions and the experimental photocurrent measurements due to the reasons discussed previously. As is seen in Supplementary Figure S6, at a lower laser power of 470 μW, the measured photocurrent along the zigzag direction is only slightly larger than the dark current. This indicates that bowtie apertures do suppress transmission effectively at low laser powers. Hence, it is anticipated that higher polarization

DOI: 10.1021/acsnano.8b01660
ACS Nano XXXX, XXX, XXX−XXX

selectivity can be realized when the incident power is lower, such as in imaging.

CONCLUSIONS

In conclusion, we demonstrated enhanced photosensitivity and polarization selectivity of black phosphorus photodetectors using resonant plasmonic structures. In the first design using bowtie antennas, we obtained an enhancement of 70% in the photoresponse in comparison to a device without plasmonic structures. The responsivity of the bowtie antenna BP photodetector, even at lower bias, is more than 4 times greater than previously reported values. Simulation shows that absorption is increased due to the field enhancement by the plasmonic structures. In the second design using bowtie apertures, photocurrent can be effectively suppressed for zigzag polarization, particularly when the incident power is low such as in imaging. An armchair to zigzag photocurrent ratio of 8.7 has been demonstrated. Enhanced photosensitivity and polarization selectivity at near-infrared wavelengths will be useful in various applications including telecommunication, remote sensing, biological imaging, and infrared polarimetry imaging.

METHODS

Sample Preparation. BP flakes are exfoliated from bulk using Scotch tape on a SiO_2/Si substrate. The thickness of the oxide layer is 50 nm. BP flakes that are large and uniform are chosen from inspection under an optical microscope. The thickness of the flakes is characterized using AFM, and the crystal direction of BP is determined by polarized Raman spectroscopy using a HORIBA LabRAM HR800 Raman spectrometer.

Optical Property Measurements. Optical properties of the BP flakes at 1550 nm are determined by exfoliating flakes onto the glass substrate and by measuring the reflectance (R) and transmittance (T) of the flakes (shown in Supplementary Figure S9). The reflectance of each sample is measured using a reference of silver-coated mirror with known reflectivity. The optical constants are then obtained from Fresnel equations using the measured reflectance, transmittance, and thickness of the films for both armchair and zigzag directions.

Numerical Computation. Plasmonic structures are modeled using the finite element electromagnetic solver ANSYS EM 17.1 with periodic boundary conditions. The frequency-dependent optical constants for gold are taken from Johnson and Christy.[50] For BP, experimentally obtained in-plane optical constants at 1550 nm of similar thickness were used for the armchair and zigzag directions for all wavelengths. Out-of-plane dielectric constants are considered the average of armchair and zigzag directions.

Fabrication. The optimized plasmonic structures and metal contacts are fabricated onto the flakes on a SiO_2/Si substrate using standard electron beam lithography, metallization, and lift-off processes. Ti/Au (5/75 nm) metal films are prepared using e-beam evaporation.

Photocurrent Measurements. The photoresponse of the devices is measured using a Keithley 2612 system. Scanning photocurrent measurements are performed using a piezostage. All optical and electrical measurements are performed in ambient atmosphere. The samples are stored in a vacuum in between measurements to avoid BP degradation.

ASSOCIATED CONTENT

Supporting Information

The Supporting Information is available free of charge on the ACS Publications website at DOI: 10.1021/acsnano.8b01660.

Dark current of devices with and without bowtie antennas, photocurrent maps of devices with and without bowtie antenna, response time of the BP photodetector, the polarization ratio with and without bowtie structures, thickness of the BP in bowtie aperture BP photodetector, $I-V$ curve of bowtie aperture BP photodetector at 470 μW, resonant wavelength of bowtie aperture array, sensitivity of resonant wavelength to optical constants, and measurement of optical property of BP (PDF)

AUTHOR INFORMATION

Corresponding Author

*E-mail: xxu@ecn.purdue.edu.

ORCID

Peide D. Ye: 0000-0001-8466-9745

Xianfan Xu: 0000-0003-0580-4625

Author Contributions

X.X. conceived the idea and supervised the numerical analyses and experiments. P.V. led the design, fabrication, and measurements of BP photodetectors. All authors analyzed the results and cowrote the manuscript.

Notes

The authors declare no competing financial interest.

ACKNOWLEDGMENTS

This work was supported by AFOSR/NSF under the EFRI2-DARE Grant EFMA-1433459. The authors would like to thank Y. Deng for help in the fabrication process and R. Ramamurthy for the valuable discussions.

REFERENCES

(1) Geim, A. K.; Novoselov, K. S. The Rise of Graphene. *Nat. Mater.* **2007**, *6*, 183−191.

(2) Geim, A. K. Graphene: Status and Prospects. *Science* **2009**, *324*, 1530−1534.

(3) Wang, Q. H.; Kalantar-Zadeh, K.; Kis, A.; Coleman, J. N.; Strano, M. S. Electronics and Optoelectronics of Two-Dimensional Transition Metal Dichalcogenides. *Nat. Nanotechnol.* **2012**, *7*, 699−712.

(4) Jariwala, D.; Sangwan, V. K.; Lauhon, L. J.; Marks, T. J.; Hersam, M. C. Emerging Device Applications for Semiconducting Two-Dimensional Transition Metal Dichalcogenides. *ACS Nano* **2014**, *8*, 1102−1120.

(5) Radisavljevic, B.; Radenovic, A.; Brivio, J.; Giacometti, V.; Kis, A. Single-layer MoS_2 Transistors. *Nat. Nanotechnol.* **2011**, *6*, 147−150.

(6) Liu, H.; Neal, A. T.; Ye, P. D. Channel Length Scaling of MoS_2 MOSFETs. *ACS Nano* **2012**, *6*, 8563−8569.

(7) Liu, H.; Neal, A. T.; Zhu, Z.; Luo, Z.; Xu, X.; Tomanek, D.; Ye, P. D. Phosphorene: An Unexplored 2D Semiconductor With a High Hole Mobility. *ACS Nano* **2014**, *8*, 4033−4041.

(8) Keyes, R. W. The Electrical Properties of Black Phosphorus. *Phys. Rev.* **1953**, *92*, 580−584.

(9) Zhang, S.; Yang, J.; Xu, R. J.; Wang, F.; Li, W. F.; Ghufran, M.; Zhang, Y. W.; Yu, Z. F.; Zhang, G.; Qin, Q. H.; Lu, Y. R. Extraordinary Photoluminescence and Strong Temperature/Angle-Dependent Raman Responses in Few-Layer Phosphorene. *ACS Nano* **2014**, *8*, 9590−9596.

(10) Tran, V.; Soklaski, R.; Liang, Y. F.; Yang, L. Layer-Controlled Band Gap and Anisotropic Excitons in Few-Layer Black Phosphorus. *Phys. Rev. B: Condens. Matter Mater. Phys.* **2014**, *89*, 235319.

(11) Zhang, G. W.; Huang, S. Y.; Chaves, A.; Song, C. Y.; Ozcelik, V. O.; Low, T.; Yan, H. G. Infrared Fingerprints of Few-Layer Black Phosphorus. *Nat. Commun.* **2017**, *8*, 14071.

(12) Iyer, V.; Ye, P. D.; Xu, X. Mid-infrared Ultrafast Carrier Dynamics in Thin Film Black Phosphorus. *2D Mater.* **2017**, *4*, 021032.

(13) Mak, K. F.; Lee, C.; Hone, J.; Shan, J.; Heinz, T. F. Atomically Thin MoS_2: A New Direct-Gap Semiconductor. *Phys. Rev. Lett.* **2010**, *105*, 136805.

DOI: 10.1021/acsnano.8b01660
ACS Nano XXXX, XXX, XXX−XXX

(14) Splendiani, A.; Sun, L.; Zhang, Y. B.; Li, T. S.; Kim, J.; Chim, C. Y.; Galli, G.; Wang, F. Emerging Photoluminescence in Monolayer MoS_2. *Nano Lett.* **2010**, *10*, 1271−1275.
(15) Li, L. K.; Yu, Y. J.; Ye, G. J.; Ge, Q. Q.; Ou, X. D.; Wu, H.; Feng, D. L.; Chen, X. H.; Zhang, Y. B. Black Phosphorus Field-Effect Transistors. *Nat. Nanotechnol.* **2014**, *9*, 372−377.
(16) Buscema, M.; Groenendijk, D. J.; Blanter, S. I.; Steele, G. A.; van der Zant, H. S. J.; Castellanos-Gomez, A. Fast and Broadband Photoresponse of Few-Layer Black Phosphorus Field-Effect Transistors. *Nano Lett.* **2014**, *14*, 3347−3352.
(17) Yang, L. M.; Qiu, G.; Si, M. W.; Charnas, A. R.; Milligan, C. A.; Zemlyanov, D. Y.; Zhou, H.; Du, Y. C.; Lin, Y. M.; Tsai, W.; Paduano, Q.; Snure, M.; Ye, P. D. Few-Layer Black Phosporous PMOSFETs with BN/Al_2O_3 Bilayer Gate Dielectric: Achieving I-on = 850 μA/μm, g(m)=340 μS/μm, and Rc = 0.58 kΩ.μm. *IEEE Int. Electron Devices Meet.* **2016**, 127−130.
(18) Bai, L. Y.; Sun, L. Q.; Wang, Y.; Liu, Z. Z.; Gao, Q.; Xiang, H. J.; Xie, H. M.; Zhao, Y. L. Solution-Processed Black Phosphorus/PCBM Hybrid Heterojunctions for Solar Cells. *J. Mater. Chem. A* **2017**, *5*, 8280−8286.
(19) Engel, M.; Steiner, M.; Avouris, P. Black Phosphorus Photodetector for Multispectral, High-Resolution Imaging. *Nano Lett.* **2014**, *14*, 6414−6417.
(20) Guo, Q. S.; Pospischil, A.; Bhuiyan, M.; Jiang, H.; Tian, H.; Farmer, D.; Deng, B. C.; Li, C.; Han, S. J.; Wang, H.; Xia, Q. F.; Ma, T. P.; Mueller, T.; Xia, F. N. Black Phosphorus Mid-Infrared Photodetectors with High Gain. *Nano Lett.* **2016**, *16*, 4648−4655.
(21) Gobin, A. M.; Lee, M. H.; Halas, N. J.; James, W. D.; Drezek, R. A.; West, J. L. Near-Infrared Resonant Nanoshells for Combined Optical Imaging and Photothermal Cancer Therapy. *Nano Lett.* **2007**, *7*, 1929−1934.
(22) Razeghi, M.; Nguyen, B. M. Advances in Mid-Infrared Detection and Imaging: a Key Issues Review. *Rep. Prog. Phys.* **2014**, *77*, 082401.
(23) Liu, Y. D.; Ang, K. W. Monolithically Integrated Flexible Black Phosphorus Complementary Inverter Circuits. *ACS Nano* **2017**, *11*, 7416−7423.
(24) Buscema, M.; Groenendijk, D. J.; Steele, G. A.; van der Zant, H. S. J.; Castellanos-Gomez, A. Photovoltaic Effect in Few-Layer Black Phosphorus PN junctions Defined by Local Electrostatic Gating. *Nat. Commun.* **2014**, *5*, 4651.
(25) Ye, L.; Li, H.; Chen, Z. F.; Xu, J. B. Near-Infrared Photodetector Based on MoS_2/Black Phosphorus Heterojunction. *ACS Photonics* **2016**, *3*, 692−699.
(26) Yuan, H. T.; Liu, X. G.; Afshinmanesh, F.; Li, W.; Xu, G.; Sun, J.; Lian, B.; Curto, A. G.; Ye, G. J.; Hikita, Y.; Shen, Z. X.; Zhang, S. C.; Chen, X. H.; Brongersma, M.; Hwang, H. Y.; Cui, Y. Polarization-Sensitive Broadband Photodetector Using a Black Phosphorus Vertical P-N Junction. *Nat. Nanotechnol.* **2015**, *10*, 707−713.
(27) Liu, Y.; Cheng, R.; Liao, L.; Zhou, H. L.; Bai, J. W.; Liu, G.; Liu, L. X.; Huang, Y.; Duan, X. F. Plasmon Resonance Enhanced Multicolour Photodetection by Graphene. *Nat. Commun.* **2011**, *2*, 579.
(28) Echtermeyer, T. J.; Britnell, L.; Jasnos, P. K.; Lombardo, A.; Gorbachev, R. V.; Grigorenko, A. N.; Geim, A. K.; Ferrari, A. C.; Novoselov, K. S. Strong Plasmonic Enhancement of Photovoltage in Graphene. *Nat. Commun.* **2011**, *2*, 458.
(29) Miao, J. S.; Hu, W. D.; Jing, Y. L.; Luo, W. J.; Liao, L.; Pan, A. L.; Wu, S. W.; Cheng, J. X.; Chen, X. S.; Lu, W. Surface Plasmon-Enhanced Photodetection in Few Layer MoS_2 Phototransistors with Au Nanostructure Arrays. *Small* **2015**, *11*, 2392−2398.
(30) Xia, F. N.; Wang, H.; Jia, Y. C. Rediscovering Black Phosphorus as an Anisotropic Layered Material for Optoelectronics and Electronics. *Nat. Commun.* **2014**, *5*, 4458.
(31) Luo, Z.; Maassen, J.; Deng, Y. X.; Du, Y. C.; Garrelts, R. P.; Lundstrom, M. S.; Ye, P. D.; Xu, X. Anisotropic In-Plane Thermal Conductivity Observed in Few-Layer Black Phosphorus. *Nat. Commun.* **2015**, *6*, 8572.
(32) Low, T.; Roldan, R.; Wang, H.; Xia, F. N.; Avouris, P.; Moreno, L. M.; Guinea, F. Plasmons and Screening in Monolayer and Multilayer Black Phosphorus. *Phys. Rev. Lett.* **2014**, *113*, 106802.
(33) Qiao, J. S.; Kong, X. H.; Hu, Z. X.; Yang, F.; Ji, W. High-Mobility Transport Anisotropy and Linear Dichroism in Few-Layer Black Phosphorus. *Nat. Commun.* **2014**, *5*, 4475.
(34) Low, T.; Rodin, A. S.; Carvalho, A.; Jiang, Y. J.; Wang, H.; Xia, F. N.; Neto, A. H. C. Tunable Optical Properties of Multilayer Black Phosphorus Thin Films. *Phys. Rev. B: Condens. Matter Mater. Phys.* **2014**, *90*, 075434.
(35) Kinzel, E. C.; Xu, X. Extraordinary Infrared Transmission Through a Periodic Bowtie Aperture Array. *Opt. Lett.* **2010**, *35*, 992−994.
(36) Nordin, G. P.; Meier, J. T.; Deguzman, P. C.; Jones, M. W. Micropolarizer Array for Infrared Imaging Polarimetry. *J. Opt. Soc. Am. A* **1999**, *16*, 1168−1174.
(37) Flores, E.; Ares, J. R.; Castellanos-Gomez, A.; Barawi, M.; Ferrer, I. J.; Sanchez, C. Thermoelectric Power of Bulk Black-Phosphorus. *Appl. Phys. Lett.* **2015**, *106*, 022102.
(38) Zhang, Y. W.; Li, H.; Wang, L.; Wang, H. M.; Xie, X. M.; Zhang, S. L.; Liu, R.; Qiu, Z. J. Photothermoelectric and Photovoltaic Effects Both Present in MoS_2. *Sci. Rep.* **2015**, *5*, 7938.
(39) Xu, X. D.; Gabor, N. M.; Alden, J. S.; van der Zande, A. M.; McEuen, P. L. Photo-Thermoelectric Effect at a Graphene Interface Junction. *Nano Lett.* **2010**, *10*, 562−566.
(40) St-Antoine, B. C.; Menard, D.; Martel, R. Position Sensitive Photothermoelectric Effect in Suspended Single-Walled Carbon Nanotube Films. *Nano Lett.* **2009**, *9*, 3503−3508.
(41) DeBorde, T.; Aspitarte, L.; Sharf, T.; Kevek, J. W.; Minot, E. D. Photothermoelectric Effect in Suspended Semiconducting Carbon Nanotubes. *ACS Nano* **2014**, *8*, 216−221.
(42) Deng, Y. X.; Luo, Z.; Conrad, N. J.; Liu, H.; Gong, Y. J.; Najmaei, S.; Ajayan, P. M.; Lou, J.; Xu, X.; Ye, P. D. Black Phosphorus-Monolayer MoS_2 Van Der Waals Heterojunction P-N Diode. *ACS Nano* **2014**, *8*, 8292−8299.
(43) Chen, Z. F.; Li, X. M.; Wang, J. Q.; Tao, L.; Long, M. Z.; Liang, S. J.; Ang, L. K.; Shu, C.; Tsang, H. K.; Xu, J. B. Synergistic Effects of Plasmonics and Electron Trapping in Graphene Short-Wave Infrared Photodetectors with Ultrahigh Responsivity. *ACS Nano* **2017**, *11*, 430−437.
(44) Chen, Z. F.; Cheng, Z. Z.; Wang, J. Q.; Wan, X.; Shu, C.; Tsang, H. K.; Ho, H. P.; Xu, J. B. High Responsivity, Broadband, and Fast Graphene/Silicon Photodetector in Photoconductor Mode. *Adv. Opt. Mater.* **2015**, *3*, 1207−1214.
(45) Knight, M. W.; Sobhani, H.; Nordlander, P.; Halas, N. J. Photodetection with Active Optical Antennas. *Science* **2011**, *332*, 702−704.
(46) Youngblood, N.; Li, M. Ultrafast Photocurrent Measurements of a Black Phosphorus Photodetector. *Appl. Phys. Lett.* **2017**, *110*, 051102.
(47) Fang, Z. Y.; Wang, Y. M.; Liu, Z.; Schlather, A.; Ajayan, P. M.; Koppens, F. H. L.; Nordlander, P.; Halas, N. J. Plasmon-Induced Doping of Graphene. *ACS Nano* **2012**, *6*, 10222−10228.
(48) Giovannetti, G.; Khomyakov, P. A.; Brocks, G.; Karpan, V. M.; Van Den Brink, J.; Kelly, P. J. Doping Graphene with Metal Contacts. *Phys. Rev. Lett.* **2008**, *101*, 026803.
(49) Wang, L.; Xu, X. Spectral Resonance of Nanoscale Bowtie Apertures in Visible Wavelength. *Appl. Phys. A: Mater. Sci. Process.* **2007**, *89*, 293−297.
(50) Johnson, P. B.; Christy, R. W. Optical Constants of Noble Metals. *Phys. Rev. B* **1972**, *6*, 4370−4379.

DOI: 10.1021/acsnano.8b01660
ACS Nano XXXX, XXX, XXX−XXX